Chemistry & Biology, Vol. 11, 1205–1215, September, 2004, ©2004 Elsevier Ltd. All rights reserved. DOI 10.1016/j.chembiol.2004.06.008

Nonspanning Bivalent Ligands as Improved Surface Receptor Binding Inhibitors of the Cholera Toxin B Pentamer

Jason C. Pickens,[1,4,5] Daniel D. Mitchell,[2,4,5] Jiyun Liu,[1,4] Xiaojian Tan,[2,4] Zhongsheng Zhang,[2,4] Christophe L.M.J. Verlinde,[2,4] Wim G.J. Hol,[2,3,4,*] and Erkang Fan[2,4,*]

[1]Department of Chemistry
[2]Department of Biochemistry
[3]Howard Hughes Medical Institute
[4]Biomolecular Structure Center
University of Washington
Seattle, Washington 98195

Summary

A series of bivalent ligands of varying length were synthesized to inhibit the receptor-binding process of cholera toxin. Competitive surface receptor binding assays showed that significant potency gains relative to the constituent monovalent ligands were achieved independently from the ability of the extended bivalent ligands to span binding sites within the toxin pentamer. Several models that could account for the unexpected improvement in IC_{50} values are examined, taking into account crystallographic analysis of each ligand in complex with the toxin pentamer. Evidence is presented that steric blocking at the receptor binding surface may play a role. The results of our study suggest that the use of relatively short, "nonspanning" bivalent ligands, or monovalent ligands of similar topology and bulk may be an effective way of blocking the interaction of multimeric proteins with their cell surface receptors.

Introduction

Multivalent ligands are an emerging theme in drug design [1, 2]. One of the hallmarks of multivalent binding is enhanced binding affinity relative to corresponding monovalent interactions. This is generally considered to be a result of the free energy savings associated with paying the penalty for the loss of overall rotational and translational entropy only once for a multivalent compound, rather than paying this penalty for each of the corresponding number of monovalent binding events. Several models for the analysis of the thermodynamic parameters associated with multivalent ligand binding have been proposed recently [3–5]. In addition, some multivalent ligands, such as those targeting lectins like concanavalin A, have been shown to act primarily through a ligand-induced clustering or aggregation effect [6, 7].

Bivalent ligands represent the simplest class of multivalent ligand. Additionally, their smaller size and increased synthetic accessibility have made them more common in drug development programs [8–13]. Examples of bivalent ligands targeting multimeric proteins are more rare and include a study by Glick et al. [14] focusing on the inhibition of influenza virus binding to immobilized sialic acid residues by bivalent sialic acid derivatives, as well as more recent studies by both Kitov et al. [15] and Lundquist et al. [16] where bivalent antagonists of Shiga-like toxin (SLT) pentamers were characterized. In the latter two cases, bivalent ligands were characterized that were able to span the distance between two closely spaced binding sites within a single subunit of the SLT pentamer.

The rationale behind the design of the bivalent ligands described in this report was influenced by results from our previous line of investigation. Specifically, we have been engaged in an overall effort to create high-affinity multivalent ligands targeting cholera toxin and heat-labile enterotoxin. Cholera toxin (CT) and heat-labile enterotoxin (LT) are two closely related AB_5 bacterial toxins that negatively affect the health of humans [17, 18]. CT is produced by *Vibrio cholerae*, the causative agent of the disease cholera. LT is produced by certain strains of pathogenic *Escherichia coli* and is known to cause traveler's diarrhea and children's diarrhea. Binding to the ganglioside GM1 receptor in the small intestine is a critical first step in the pathway leading to the toxic effects of these proteins [19]. As such, developing high affinity ligands that block the interaction between GM1 and these protein toxins is an attractive route to preventing the severe diarrhea stemming from infection with *V. cholerae* or enterotoxigenic *E. coli*. Moreover, such surface receptor binding inhibitors do not have to pass any membranes to exert their effect. Hence, they can be virtually any size and carry substantial charge.

Previous multivalent constructs studied by us include both pentavalent and branched pentavalent (or decavalent) ligands [20–22]. The most potent of these compounds has an IC_{50} around 40 nM in an in vitro competitive binding assay. Furthermore, the decavalent ligands were found to be substantially better at inhibiting receptor binding ($\sim$10-fold) than the corresponding pentavalent ligands. Thus, one conclusion that can be drawn from these studies is that the improvement in IC_{50} displayed by the decavalent ligands must be due to a substantial difference in affinity between the galactose fragment within the pentavalent ligand and the rather short, nonspanning bivalent galactose moiety within the decavalent ligand. This prompted us to further investigate the properties of short, nonspanning bivalent ligands as surface receptor binding inhibitors of CT and LT.

This report describes a set of novel bivalent ligands targeting the B pentamer of cholera toxin and heat-labile enterotoxin. All of the compounds are too short to effectively span the distance between any two binding sites within the toxin's B pentamer. Hence, we refer to such compounds as "nonspanning" bivalent ligands. We found, somewhat unexpectedly, that substantial gains in *surface* receptor binding inhibition relative to the constituent monovalent ligands was achieved independently from the ability of the bivalent ligand to span

*Correspondence: erkang@u.washington.edu; wghol@u.washington.edu
[5]These authors contributed equally to this work.

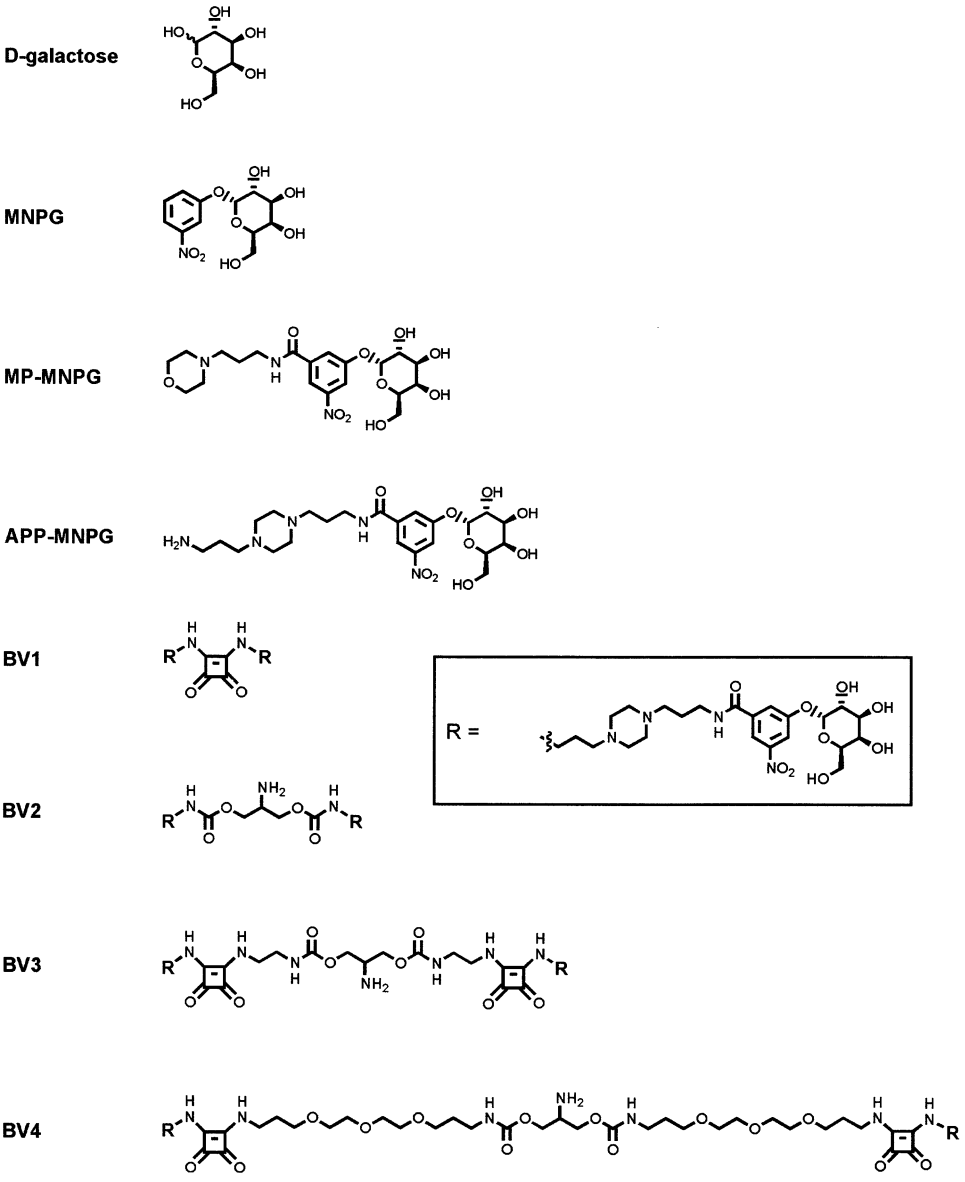

Figure 1. Previously Studied Monovalent Ligands to CT and LT and Chemical Structure of Newly Synthesized Bivalent Ligands BV1–BV4

binding sites within the toxin pentamer, a system distinctly different from those for which models were developed [3–7]. Consequently, the results presented here may have substantial implications for the design of bioactive compounds that target cell surface receptor binding processes.

Results

Ligand Design

The set of bivalent ligands presented here was based on monovalent compounds with much higher affinity for the toxin pentamer than a simple D-galactose moiety. We recently described the synthesis and characterization of a number of improved monovalent ligands derived from the commercially available compound *m*-nitrophenyl-α-D-galactopyranoside (MNPG, Figure 1) [23, 24]. In an early study, MNPG was found to display a 100-fold increase in affinity relative to D-galactose. Aided by the crystal structure of this compound bound to CTB_5 and LTB_5, MNPG was used as a scaffold in the design of subsequent series of monovalent antagonists. The first was a collection of 15 compounds incorporating a small diverse set of ring systems through an alkyl benzamide linkage *meta* to the nitro group of MNPG. The morpholine-ring-containing compound (3-nitro-5-(3-morpholin-4-yl-propylaminocarbonyl)phenyl)-α-D-galactopyranoside (MP-MNPG, Figure 1), having good aqueous solubility and an additional 14-fold affinity gain over MNPG, was then used in the design and synthesis of the second series of compounds culminating in the synthesis of N-{3-[4-(3-amino-propyl)-piperazin-1-yl]-propyl}-3-nitro-5-(3,4,5-trihydroxy-6-hydroxymethyl-tetrahydro-pyran-2-yloxy)-benzamide (APP-MNPG) of Figure 1 [25]. This compound features a propylpiperazine group that serves as an isosteric replacement of

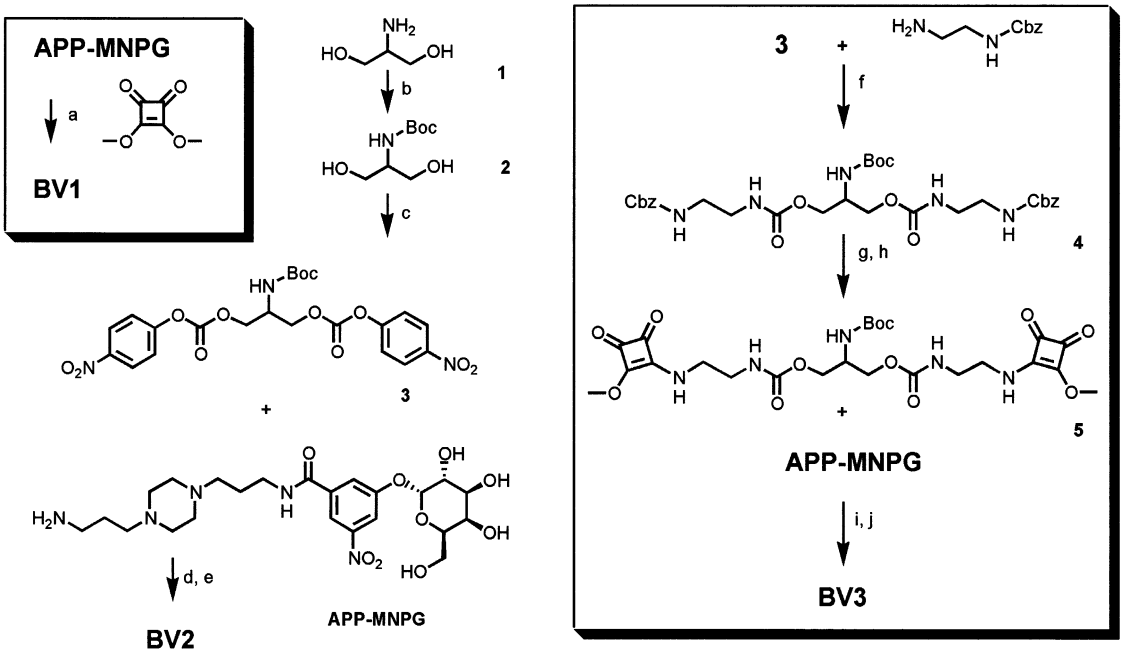

Figure 2. Synthesis of BV1–BV3

Conditions: (a) MeOH/H_2O (pH 9.0); (b) di-*t*-butyl-dicarbonate, EtOH, 4°C; (c) *p*-nitrophenylchloroformate, CH_2Cl_2; (d) DIEA/DMF; (e) 1:1 TFA/CH_2Cl_2, 30 min; (f) dilute 3 in CH_2Cl_2 added dropwise to *N*-(2-aminoethyl)-carbamate hydrochloride in DMF, 22°C; (g) H_2 (1 atm) Pd/C (10%) in EtOH; (h) excess dimethyl squarate, MeOH/H_2O (pH 7.0); (i) MeOH/H_2O (pH 9.0); (j) 1:1 TFA/CH_2Cl_2, 30 min.

the propylmorpholine moiety of MP-MNPG, and at the same time provided an additional short linker terminating in a primary amine through which the compound can be further modified. The IC_{50} of APP-MNPG alone is around 350 μM making it our most potent monovalent compound with good aqueous solubility so far. Thus, we chose to incorporate APP-MNPG into the current series of bivalent ligands.

The structures of the newly synthesized compounds are shown in Figure 1. BV1 is the shortest of the series and contains a central squarate ring. BV2, BV3, and BV4 have longer, flexible linkers emanating from both ends of 2-amino-1,3-propanediol via carbamate linkages. We chose the 2-amino-1,3-propanediol as the central element of the bivalent ligand because it provides a primary amine that can be used in later conjugation to multivalent scaffolds if desired. Both BV3 and BV4 contain the squarate linkage between the propylpiperazine of APP-MNPG and the internal variable-length linker. In the case of BV2, the propylpiperazine is coupled directly into the carbamate linkage. Using an empirical formula for estimating the effective end-to-end length of a linear poly(ethylene glycol) chain in solution [26], we estimated the *effective* length between the two MNPG moieties of BV1–BV4 to be 17 Å, 19 Å, 22 Å, and 27 Å, respectively. *Extended* lengths were determined to be 29 Å, 35 Å, 48 Å and 73 Å, respectively for BV1–BV4. The calculation of effective and extended lengths was carried out for comparison to the 35 Å distance between adjacent binding sites within the toxin B pentamer.

Synthesis of Bivalent Ligands

The synthesis of BV1–BV4 is depicted in Figures 2 and 3. BV1 was obtained by treating APP-MNPG with 0.5 equivalents of dimethyl squarate under basic conditions using previously reported conditions [20]. In our hands, the formation of the squaryl diamide proceeds efficiently under the conditions employed without the need for sugar protecting groups. The synthesis of BV2 and BV3 was slightly more involved (Figure 2). Starting from 2-amino-1,3-propanediol (**1**) the amino group was protected with Boc using di-*t*-butyl-dicarbonate in dioxane to give **2**. Subsequent reaction with an excess of *p*-nitrophenyl chloroformate in dichloromethane gave the previously reported bis-nitrophenylcarbonate **3** [22]. This compound was then reacted with an excess of APP-MNPG in DMF in the presence of N,N-diisopropylethyl amine (DIEA) to give Boc-protected BV2 which was then treated with 1:1 TFA/CH_2Cl_2 yielding the free amine. HPLC purification followed.

The synthesis of BV3 was the same as for BV2 through intermediate **3** which was then treated with the commercially available benzyl *N*-(2-aminoethyl)-carbamate hydrochloride to give the orthogonally protected intermediate **4**. The Cbz protecting groups of **4** were removed by hydrogenolysis quantitatively over 10 percent palladium on activated charcoal. The resulting diamine intermediate was then immediately brought up in methanol containing an excess of dimethyl squarate under neutral conditions to give **5** after HPLC. Treatment of **5** with an excess of APP-MNPG under basic aqueous conditions gave Boc-protected BV3, which was deprotected and purified in a manner analogous to BV2.

For the synthesis of BV4 (Figure 3), compound **3** was treated with a large excess of the diamine 4,7,10-trioxa-1,13-tridecanediamine to give the crude diamine intermediate **6** after extractive work-up. The rest of the synthesis was performed in a manner analogous to that of

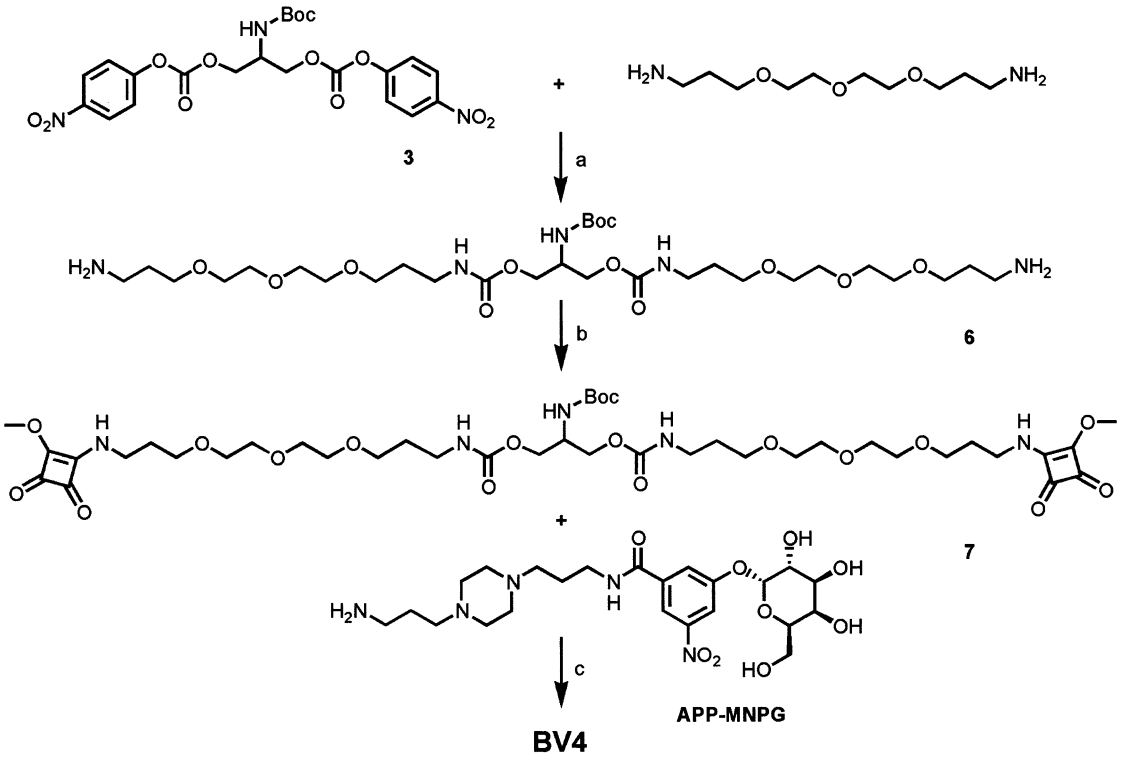

Figure 3. Synthesis of BV4

Conditions: (a) Dropwise addition of 3 to neat 4,7,10-trioxa-1,13-tridecanediamine; (b) excess dimethyl squarate, MeOH/H_2O (pH 7.0); (c) (i) MeOH/H_2O (pH 9.0) (ii) 1:1 TFA/CH_2Cl_2, 30 min.

BV3 after the removal of Cbz groups. In both cases, HPLC purification of intermediates **5** and **7** was necessary to remove excess dimethyl squarate and other accumulated impurities.

IC_{50} Values

The four compounds BV1–BV4 were tested using a competitive GD_{1b} surface receptor binding assay, a CT-HRP direct enzyme-linked assay (CT-DELA) [23]. Binding curves for the bivalent compounds are shown in Figure 4 along with those previously obtained for MNPG and APP-MNPG for comparison. From these curves, it is clear that all of the bivalent ligands are much better at blocking CT conjugate binding to the GD_{1b}-coated microtitre plate surface compared to MNPG or APP-MNPG. IC_{50} values for the series range from roughly 10 to 30 μM compared to 338 μM for APP-MNPG and 1700 μM for MNPG, our previous benchmark lead. With respect to the most potent compound BV3, having an IC_{50} of 9 μM, this corresponds to an improvement over APP-MNPG and MNPG of around 35- and 200-fold, respectively.

Crystallographic Analysis

As a first step toward better understanding of the lack of dependence on the linker length evident in the IC_{50} values, X-ray crystal structures of all four bivalent compounds bound to CTB_5 were determined at high resolution. Crystals of space group C2 were obtained from sitting drop experiments under conditions similar to those previously reported for the crystallization of APP-MNPG and related compounds [25]. Data collected at

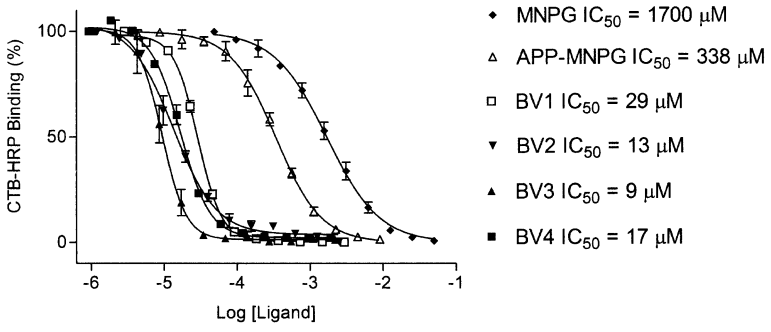

Figure 4. Binding Curves and IC_{50} Values

Error bars represent the standard error of the mean for at least two independent determinations.

Table 1. Crystallographic Data Collection and Refinement Statistics

Data Collection Statistics	CTB5 + BV1	CTB5 + BV2	CTB5 + BV3	CTB5 + BV4
Source	ALS 8.2.2	ALS 8.2.2	ALS 8.2.2	ALS 8.2.2
Wavelength (Å)	1.0000	1.0000	0.9791	0.9626
Resolution (Å)	1.60	1.44	1.35	1.35
Space group	C2	C2	C2	C2
Number of observations	227,195	297,752	368,119	365,261
Unique reflections	63,041	81,971	100,384	104,314
Completeness (%)	96.0 (76.3)	92.4 (73.3)	91.3 (63.8)	94.2 (69.3)
$<I/\sigma(I)>$	18.3 (3.0)	14.4 (1.9)	19.5 (2.4)	13.5 (1.8)
R_{merge}	6.4 (37.1)	8.3 (56.7)	5.9 (45.1)	8.1 (59.1)
Refinement Statistics				
Number of residues	515	515	515	515
Water molecules	466	491	494	498
Bivalent ligand molecules	5	5	5	5
Other molecules	None	1 TRIS, PEG	1 TRIS, PEG	1 TRIS, PEG
Ligand atoms - Site D	24	24	24	24
Ligand atoms - Site E	36	37	24	24
Ligand atoms - Site F	24	24	24	24
Ligand atoms - Site G	24	24	24	24
Ligand atoms - Site H	24	37	24	24
R_{cryst} (outer)	0.164 (0.217)	0.131 (0.192)	0.130 (0.208)	0.132 (0.236)
R_{free} (outer)	0.193 (0.270)	0.184 (0.293)	0.171 (0.281)	0.174 (0.304)
Figure of merit	0.879	0.888	0.893	0.892
RMSD from ideal				
Bond lengths (Å)	0.013	0.013	0.013	0.012
Angles (°)	1.5	1.4	1.5	1.4
Chirality	0.097	0.092	0.088	0.086

the Advanced Light Source (ALS) provided data sets for all four complexes at resolution ranging from 1.35 Å to 1.60 Å. Data collection and refinement statistics are shown in Table 1.

All of the crystals were in space group C2 yielding structures that contained one B pentamer in the asymmetric unit and thus five unique views of the binding site. In all of the binding sites of all of the structures, very clear electron density is seen corresponding to the galactose ring and nitrobenzamide moiety. Furthermore, in all the binding sites, the binding mode of the nitrophenyl galactoside is identical to that seen for MNPG [27] and APP-MNPG [25], where canonical water #2 is displaced from the binding site. To varying degrees, additional density is seen that corresponds to the piperazine ring and its aminopropyl extension. More importantly, no discernable electron density is visible in any of the structures corresponding to the linker, or to a second copy of the nitrophenyl galactose bound at a subsite on the protein. In a few cases, extra density is visible corresponding to other components of the crystallization solution. A more detailed description of the electron density seen in each cocrystal structure follows.

The cocrystal structure of CTB_5 and BV1 was determined at a resolution of 1.60 Å. In addition to the very clear density corresponding to the galactoside portion of the ligand, all five binding sites show additional density above Tyr12 corresponding to the aminopropyl piperizine moiety. In four out of the five binding sites, the electron density is not strong enough to construct a precise model. In the remaining site, enough electron density is available to warrant building a more complete model including the piperazine ring and the propyl linkers (Figure 5A). The piperazine ring itself rests in a small, shallow pocket formed between Glu11 and the face of Tyr12. Interactions between the protein and the piperazine ring in this region appear to be nonspecific, allowing for multiple binding modes.

The cocrystal structure of CTB_5 with BV2 was solved at a resolution of 1.44 Å. In all five binding sites, strong density corresponding to the nitrophenyl galactoside is clearly visible. As before, there is additional density to varying degrees in each of the binding sites at the piperazine binding pocket (not shown). In two of the binding sites, the density is strong enough to support a model that includes the aminopropyl piperazine as before. In this structure, extra density is seen in two places at the crystal-packing interface along one edge of the pentamer. One of these extra regions of density was a molecule of tris(hydroxymethyl)aminoethane (TRIS buffer) and the other a segment of poly(ethylene glycol) (PEG) which was also present in the crystallization drop. The TRIS model fits the electron density very well with its primary amine nitrogen forming a hydrogen bond with Glu11 2.72 Å away, and a water molecule 3.14 Å away. The other piece of extra density modeled as a segment of PEG extends 5–9 Å between two symmetry-related pentamers.

The two cocrystal structures of CTB_5 with BV3 and with BV4 were both determined at a resolution of 1.35 Å. Electron density corresponding to the nitrophenylgalactoside portion of the ligand was seen and modeled into all five binding sites in both cases. Very little additional density was seen corresponding to the piperazine ring in any of the five sites of the BV4 structure (Figure 5B). Some additional density was seen in the piperazine pocket in the BV3 structure, but not enough to justify

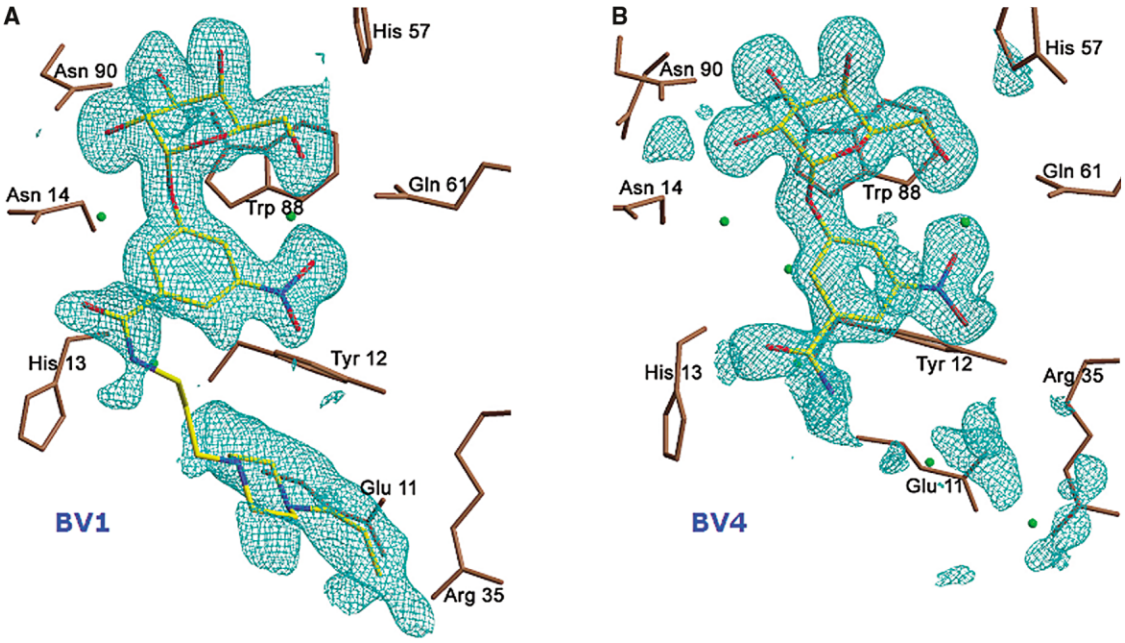

Figure 5. Electron Density and Fitted Model

(A) Electron density and model for BV1 in complex with CTB_5. Electron density is contoured at 2σ in a σ_A-weighted (mFo–DFc) difference map.
(B) Electron density and model for BV4 in complex with CTB_5. Electron density is contoured at 3σ in a σ_A-weighted (mFo-DFc) difference map.

modeling beyond the nitrobenzamide ring. Both structures had similar extra density to that seen in the BV2 structure that was again modeled as a molecule of TRIS from the buffer and a fragment of PEG. Hence, the crystal structures containing BV3 and BV4, compounds that could potentially span two binding sites if their linkers were substantially stretched out, do not provide any evidence for such behavior.

Discussion

Given the fact that the effective linker lengths for the series range from 17 Å, in the case of BV1, to roughly 27 Å in the case of BV4, the substantial improvement in IC_{50} displayed by the bivalent compounds independent of their respective linker lengths (Figure 4) is quite unexpected and intriguing since the distance between adjacent binding sites is 35 Å (Figure 6). Several scenarios exist that might account for this increased potency including the following: (1) favorable interactions between the linker and/or pendant sugar portion of the ligands with the protein surface, (2) intermolecular cross-linking of toxin pentamers during the incubation step of the competitive binding assay, (3) avidity-based enhancements due to bivalent binding of the ligand within a single pentamer, (4) electrostatic effects and, (5) steric blocking effects in the competitive surface binding assay. Each of these possibilities is examined in the following discussion.

Based on the fact that no electron density is seen in any of the crystal structures corresponding to the linker or pendant sugar, one may conclude that additional favorable interactions involving these portions of the bivalent ligand with the protein are not a primary reason for the improvement in IC_{50} values for the bivalent series. This is not meant to imply that transient, nonspecific interactions between the linker and the protein in solution are impossible. However, this would be very difficult to test experimentally and would still fail to account for the collective improvement in IC_{50} of all the compounds tested because the structure and length of the linkers vary substantially. Also, a subsite for the pendant sugar seems an unlikely explanation as well because the existence of a such a subsite for the galactose moiety has not yet been seen in any previous crystal structures of the toxin B pentamer in complex with a variety of monovalent or multivalent ligands, including those containing D-galactose alone at high concentration [17, 28].

Intermolecular cross-linking and subsequent formation of aggregates and/or clusters is another possibility that has been shown to play a significant role in other systems, such as the binding of concanavalin A to multivalent displays of mannose [6, 7]. In our current assay system, the total concentration of ligand at the IC_{50} is present at a 10^5 molar excess over the CT-HRP conjugate, which is held at a constant concentration of around 100 pM. Hence, intermolecular cross-linking of toxin pentamers under these conditions is very unlikely. Unfortunately, these very dilute conditions can't be employed within the detection limits of dynamic light scattering (DLS) experiments, which would allow one to rigorously test this assumption. However, preliminary DLS studies of the best bivalent compound, BV3, together with the B pentamer both at much higher concentrations (10–50 μM) than employed in the assay indicated that very little of the bulk sample contained species larger than the B pentamer alone. Additionally, we have previously shown very clearly by DLS measurements that

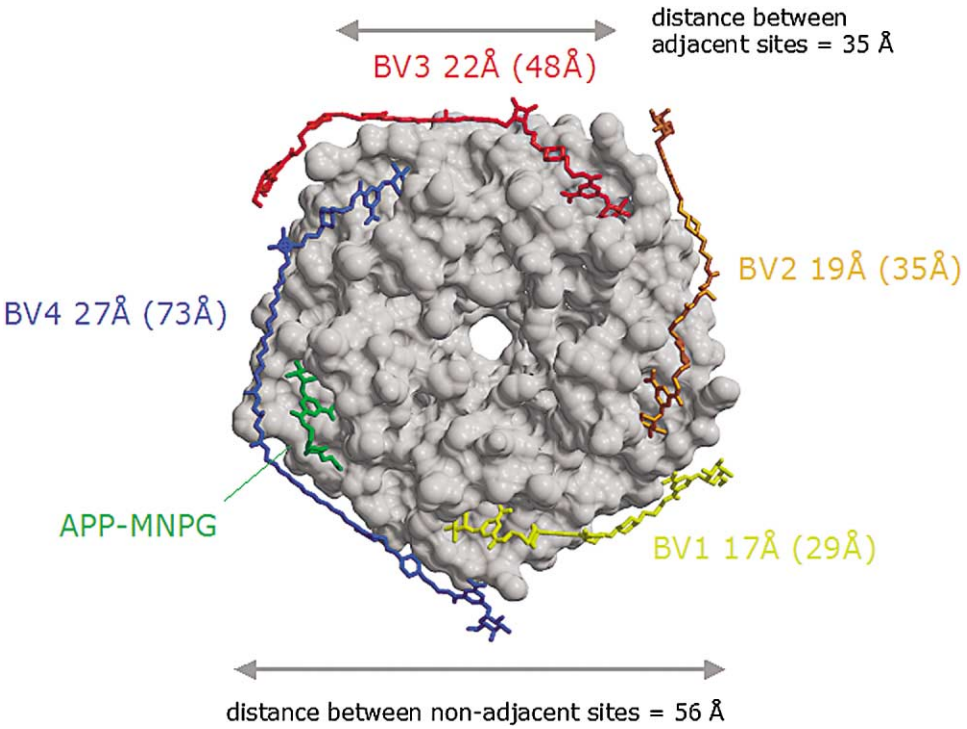

Figure 6. Relative Dimension of CTB_5 and BV1–BV4

Effective linker lengths between MNPG amide group nitrogen atoms were determined in a manner described previously [26] and are listed beside the compound labels. Values in parentheses indicate extended linker lengths from the same end point atoms. Nonenergy-minimized models for each bivalent ligand were constructed starting from the structure of APP-MNPG (green) bound to CTB_5 [25]. Figure made using *RASTER3D* [40].

ligand-induced cross-linking is not a large component of the binding between the toxin pentamers and any of the much more potent pentavalent and decavalent ligands under conditions where the ligand is held in great excess [20–22].

Enhancements from intramolecular, bivalent binding of the ligands are a third possibility (Figure 6). However, despite the fact that the shortest distance between two adjacent binding sites is only 35 Å, the radial symmetry of the pentamer, combined with a convoluted protein surface path, allows only the longest compound, BV4 in an extended form, to present a pendant copy of the galactoside to an adjacent binding site without substantial conformational restriction of the linker. It should be noted, however, that the 27 Å effective linker length of BV4 is still significantly shorter than the distance of 35 Å between adjacent binding sites within the B pentamer. Since the IC_{50} of BV4 is not dramatically different from the other bivalent ligands including even BV1, one may conclude that the ability to span two binding sites alone is not a major contributor to the IC_{50} improvement displayed by the series as a whole.

Electrostatic effects should be considered as well. Each of the bivalent ligands is expected to carry three positive charges under the nearly neutral aqueous conditions employed in the assay. Therefore, if the "bottom" surface of the toxin pentamer displayed many negatively charged residues, one could invoke electrostatic complementarity to explain the IC_{50} improvement. However, with the exception of two glutamatic acid residues in each of the five B monomers, the remaining 25 of the 35 charged residues on the bottom of the pentamer are positively charged lysines and arginines. This electrostatic anticomplementarity, along with expected attenuating effects of the high ionic strength phosphate-buffered saline solution used in the assay, render favorable electrostatic effects unlikely to be the cause of the IC_{50} improvement of the bivalent compounds over their monovalent counterparts.

A final intriguing possibility is that of steric blocking at the toxin binding surface. One could argue that when the toxin's five binding sites are partially saturated, the steric bulk of the pendant portion of the nonspanning bivalent ligands may be able to prevent close approach of the pentamer to the microtitre plate surface bearing the immobilized ganglioside, thus indirectly blocking access of the surface receptors to the unoccupied sites. Such a phenomenon would be similar to known "steric stabilization" effects reported for the large polyacrylamide-based polyvalent inhibitors of influenza virus agglutination [29–31]. Also, the pendant portion of the longer bivalent ligands may be able to sterically occlude access to unoccupied receptor binding sites. Conceivably, the combination of these two effects could drive the equilibrium of conjugate binding toward the non-plate-bound state during the incubation step of the assay, resulting in a roughly equal apparent decrease in the IC_{50} for all of the bivalent ligands. Based on this model, one would predict that very short bivalent ligands would yield the smallest potency gains. Consistent with

this prediction is the observation that the shortest bivalent ligand BV1 shows the least dramatic improvement, only 10-fold relative to compound APP-MNPG (Figure 4). Additionally, the model implies that a monovalent ligand with an analogous linker region, but missing the pendant copy of the galactoside, might be nearly as effective as the bivalent version. Experiments designed to thoroughly test this hypothesis are in progress.

In addition to examining the collective behavior of the bivalent compounds reported here, internal comparisons are also worth noting. The IC_{50} for APP-MNPG is around 350 μM, between that of the bivalent compounds (10–30 μM) and MNPG (1.7 mM). This indicates that the dipropylpiperazine moiety of APP-MNPG, and more than likely, of the bivalent ligands, is engaging in at least some favorable interactions within the GM1 binding site. This is consistent with the previous crystallographically observed binding mode of APP-MNPG bound to CTB_5, in which electron density is seen for the piperazine ring continuing through the terminal propylamine where these segments of the ligand contact the protein surface [25]. As a result, one can either describe BV1–BV4 as bivalent versions of APP-MNPG, where the dipropylpiperazine moiety is considered part of the pharmacophore, or bivalent versions of MNPG where the dipropylpiperazine is considered to be part of the linker while incidentally providing additional favorable interactions with the protein near to where the MNPG moiety is bound. Additionally, the IC_{50} values shown in Figure 4 for BV2, BV3, and BV4 differ from each other by less than a factor of two, making them essentially the same within the context of the assay format.

Significance

Diarrheal diseases such as those caused by the action of cholera toxin and the related heat-labile enterotoxin from certain pathogenic strains of *E. coli* continue to threaten the health of millions of people each year. As part of a continuing effort to create effective antagonists of toxin receptor binding, the findings described in this report reveal that the use of nonspanning bivalent ligands can produce potency gains of 10- to 100-fold beyond what would be expected from the mere presence of an additional copy of the monovalent binding element. A combination of solution and crystallographic studies were used to test various hypotheses that would account for the increased potency of the bivalent ligands. The results suggest that steric blocking may play a role in the competitive surface receptor binding inhibition. Consequently, the use of bivalent or nonbivalent compounds with similar, or even greater steric bulk than those reported here may represent an attractive general design strategy for blocking the binding capability of a variety of multimeric proteins to their cell surface receptors. The present findings are also likely to provide motivation for future studies aimed at probing the feasibility of incorporating a steric blocking element into a variety of multivalent drug design strategies.

Experimental Procedures

Synthetic Chemistry

Unless otherwise noted, commercially available reagents and solvents were used as purchased without further purification. ^{1}H-NMR spectra were recorded using a Bruker AC-300 operating at 300 MHz. Samples were dissolved in methanol-d_4 and not subjected to spinning during spectra acquisition. LC-MS characterization was performed using an Agilent 1100 series instrument equipped with a variable wavelength detector coupled to an Agilent 1100 MSD-Trap SL electrospray ion trap mass spectrometer operating in positive ion mode. Reported values for the molecular ion $[M+H]^+$ of target compounds refer to those obtained during LC-MS analysis either during or after purification. Columns used for both preparative C18 reverse-phase HPLC purification and LC-MS characterization were purchased from Agilent Technologies (Zorbax SB-AQ, 5 μm, 4.6 or 21.2 × 150 mm). Analytical and preparative HPLC purifications were performed using mixed solvent systems comprised of acetonitrile and 0.1% TFA in water at a flow rate of either 0.5 ml min^{-1} (analytical) or 30 ml min^{-1} (preparative).

N-Boc-2-amino-1,3-propanediol **(2)**. 2-amino-1,3-propanediol (2.0 g, 21.5 mmol) was dissolved in 20 ml of absolute ethanol. Di-*tert*-butyl-dicarbonate (5.6 g, 26 mmol) was dissolved in 20 ml of absolute ethanol in a 50 ml addition funnel and added dropwise to the solution of 2-amino-1,3-propanediol at 4°C over a period of one hour. The solution was then gently warmed to 37°C and stirred vigorously for another hour. The solvent was removed under vacuum and the remaining clear oil was suspended in a 1:1 solution of EtOAc and hexane. The mixture was heated until all solids were dissolved. Then, additional hexane was added until the solution became slightly cloudy. The resulting suspension was then placed in a 4°C freezer overnight to promote crystallization. Filtration gave large white flakes (3.99 g, 85% yield). ^{1}H-NMR ($CDCl_3$) δ 4.87 (br. m, 1H), 3.57 (s, CH_2, 4H), 1.44 (s, Boc, 9H).

N-Boc-2-amino-1,3-bis (4-nitrophenyloxy-carbonyloxy)propane **(3)**. Compound **3** was prepared as previously described [22].

{2-[3-(2-Benzyloxycarbonylamino-ethylcarbamoyloxy)-2-tert-butoxycarbonylamino-propoxycarbonylamino]-ethyl}-carbamic acid benzyl ester **(4)**. A solution of the dicarbonate **3** (200 mg, 0.38 mmol) in 20 ml CH_2Cl_2 was added dropwise over a period of 3 hr to a DMF solution containing benzyl-N-(2-aminoethyl)-carbamate hydrochloride (500 mg, 2.2 mmol) and 500 μl of diisopropylethylamine (DIEA). When the addition was complete, the solvent was removed under vacuum and the remaining clear residue dissolved in 5 ml of MeOH and purified by preparative HPLC to give 196 mg of **4**. Yield: 82%. ESI-MS *m/z* 632.1 $[M+H]^+$, 532.1 (-Boc). ^{1}H-NMR: δ 7.34-7.28 (m, aromatic H), 5.06 (s, 4H), 4.2-3.8 (br. m, 5H), 3.19 (s, 8H), 1.41 (s, 9H).

{2-[2-(2-methoxy-3,4-dioxo-cyclobut-1-enylamino)-ethylcarbamoyloxy]-1-[2-(2-methoxy-3,4-dioxo-cyclobut-1-enylamino)-ethylcarbamoyloxymethyl]-ethyl}-carbamic acid tert-butyl ester **(5)**. The synthesis of **5** was performed in two steps. Hydrogenolysis of Cbz groups was accomplished by stirring a solution **4** (166 mg, 0.26 mmol) in 4 ml EtOH containing approximately 200 mg of (10%) Pd/C under H_2 (1 atm) for 4.5 hr. The reaction was then checked by LC-MS that indicated when the reaction was complete. After filtration to remove the catalyst and solvent removal, 88 mg of the deprotected intermediate was obtained as clear oil. Yield: 92%. ESI-MS *m/z* 364.1 $[M+H]^+$. This material was brought up in 3 ml of MeOH along with dimethyl squarate (360 mg, ~50-fold excess) and stirred overnight. The reaction was checked by LC-MS to confirm completion and then purified by preparative HPLC under standard conditions giving 76 mg of purifed **5** as colorless syrup. Yield: 66%. ESI-MS *m/z* 584.0 $[M+H]^+$, 484.0 (–Boc).

(3-{2-[2-(3-amino-propoxy)-ethoxy]-ethoxy}-propyl)-carbamic acid 3-(3-{2-[2-(3-amino-propoxy)-ethoxy]-ethoxy}-propylcarbamoyloxy)-2-tert-butoxycarbonylamino-propyl ester **(6)**. Dicarbonate **3** (400 mg, 0.076 mmol) was added drop-wise over a period of 3 hr to 20 ml of the diamine 4,7,10-trioxa-1,13-tridecanediamine with rapid stirring. The sample was diluted with 50 ml of water and the organic layer separated. Extraction of the aqueous layer with 2 × 50 ml CH_2Cl_2 followed. The organic fractions were combined and washed with water until colorless. The solvent was dried over $MgSO_4$, filtered, and removed under vacuum to give 280 mg of a pale yellow syrup which was used directly without further purification or characterization in the synthesis of **7**. Yield: 53%.

[3-(2-{2-[3-(2-methoxy-3,4-dioxo-cyclobut-1-enylamino)-propoxy]-ethoxy}-ethoxy)-propyl]-carbamic acid 2-tert-butoxycarbonylamino-3-[3-(2-{2-[3-(2-methoxy-3,4-dioxo-cyclobut-1-enylamino)-propoxy]-ethoxy}-ethoxy)-propylcarbamoyloxy]-propyl ester **(7)**.

Compound **6** (280 mg, 0.31 mmol) was dissolved in 10 ml of MeOH. Dimethyl squarate (1.0 g, ~50-fold excess) was then added while stirring. The solution was stirred for an additional 24 hr at room temperature and then purified directly by preparative HPLC. Prior to solvent removal by rotary evaporator, the acidic aqueous fractions obtained from purification were neutralized to pH 7.0 using concentrated ammonium hydroxide to prevent removal of the Boc group. The sample was desalted using a Waters SepPak C18 cartridge. Elution from the cartridge with pure MeOH followed by solvent removal gave 167 mg of pale yellow oil (**7**). Yield: 45%. ESI-MS *m/z* 904.4 $[M+H]^+$, 804.4 (–Boc), ^{1}H-NMR: δ 4.38, 4.35 (d, 4H), 4.03 (br. m, 5H), 3.70–3.49 (m, 30H), 3.18 (t, 4H), 1.85 (quintet, 4H), 1.74 (quintet, 4H), 1.43 (s, 9H).

Bivalent compound BV1. APP-MNPG (10 mg, 0.018 mmol) and dimethyl squarate (1 mg, 0.007 mmol) were brought up in 2 ml of a solution of 1:1 aqueous $NaHCO_3$ and MeOH (pH ≥ 9). The solution was stirred at room temperature overnight. After filtration to remove any precipitated $NaHCO_3$, the solution was acidified with a drop of glacial acetic acid and subjected to HPLC purification. After removal of the solvent, the clear residue was dissolved in 1 or 2 ml of water and lyophilized to give 11 mg of BV1 as the TFA salt. Yield: 61%. ESI-MS *m/z* 1133.5 $[M+H]^+$ 567.5 $[M+2H]^{2+}$. ^{1}H-NMR: δ 8.35 (s, 2H), 8.17 (s, 2H), 8.00 (s, 2H), 5.70,5.69 (d, 2H anomeric), 4.0–3.53 (m, 14H, overlapping resonances from galactose rings), 3.51 (t, 4H), 3.05 (br. m, 8H), 2.86 (br. t, 4H), 2.01–1.91 (m, 8H).

Bivalent compound BV2. Compound **3** (5 mg, 0.010 mmol) and APP-MNPG (20 mg, 0.036 mmol) were dissolved in 250 μl of DMF in a small vial containing a micro stir bar. N,N-diisopropylethylamine (30 μL) was then added. The vial was sealed and transferred to a 37°C oven and kept stirring overnight. The sample was diluted with MeOH and checked for completion by LC-MS. Upon completion the sample was purified by preparative HPLC. After solvent removal, the clear residue was dissolved in 1 or 2 ml of water and lyophilized to give 10 mg of the Boc-protected target compound; ESI-MS *m/z* 1298.8 $[M+H]^+$, 650.1 $[M+2H]^{2+}$. Deprotection using 2 ml of 1:1 TFA/CH_2Cl_2, subsequent solvent removal and relyophilization gave 9 mg of the final compound. Yield: 79%. ESI-MS *m/z* 1198.6 $[M+H]^+$, 600.0 $[M+2H]^{2+}$. ^{1}H-NMR: δ 8.34 (s, 2H), 8.16 (s, 2H), 7.98 (s, 2H), 5.69 (s, 2H, anomeric), 4.3 (m, 4H), 4.2–3.8 (m, 6H), 3.7–3.69 (d, 4H), 3.60–3.0 (m, 35H), 2.05 (m, 4H), 1.89 (m, 4H).

Bivalent compound BV3. APP-MNPG (60 mg, 0.113 mmol) and compound **5** (12 mg, 0.020 mmol) were brought up in 2 ml of a solution of 1:1 aqueous $NaHCO_3$ and MeOH (pH ≥ 9). The solution was stirred at room temperature overnight. After filtration to remove any precipitated $NaHCO_3$, the solution was acidified with a drop of glacial acetic acid and subjected to HPLC purification. After solvent removal, the clear residue was dissolved in 1 or 2 ml of water and lyophilized to give 18 mg of Boc-protected BV3; ESI-MS *m/z* 1574.5 $[M+H]^+$, 788.0 $[M+2H]^{2+}$. Deprotection using 2 ml of 1:1 TFA/CH_2Cl_2, subsequent solvent removal and relyophilization gave 17 mg of the final compound. Yield: 56% from **5**. ESI-MS *m/z* 1476.6 $[M+H]^+$, 738.0 $[M+2H]^{2+}$. ^{1}H-NMR: δ 8.33 (s, 2H), 8.15 (s, 2H), 7.98 (s, 2H), 5.69 (s, 2H), 4.5–3.0 (br. m, 53H), 2.05 (br. m, 12H).

Bivalent compound BV4. APP-MNPG (70 mg, 0.132 mmol) and compound **7** (10 mg, 0.011 mmol) were brought up in 2 ml of a solution of 1:1 aqueous $NaHCO_3$ and MeOH (pH ≥ 9). The solution was stirred at room temperature overnight. After filtration to remove any precipitated $NaHCO_3$, the solution was acidified with a drop of glacial acetic acid and subjected to HPLC purification. After solvent removal, the clear residue was dissolved in 1 or 2 ml of water and lyophilized to give 12 mg of Boc-protected BV4; ESI-MS *m/z* 1894.8 $[M+H]^+$, 948.4 8 $[M+2H]^{2+}$. Deprotection using 2 ml of 1:1 TFA/CH_2Cl_2, subsequent solvent removal and relyophilization gave 11 mg of the final compound. Yield: 56% from **7**. ESI-MS *m/z* 1476.6 $[M+H]^+$, 738.0 $[M+2H]^{2+}$. ^{1}H-NMR: δ 8.33 (s, 2H), 8.16 (s, 2H), 7.98 (s, 2H), 5.69 (s, 2H), 4.3 (br. m, 4H), 3.97, (m, 4H), 3.85 (m, 2H), 3.8–2.8 (br. m, 77H), 2.05 (br. m, 12H), 2.8 (m, 4H), 1.74 (m, 4H).

IC_{50} Determinations

The GD1b direct enzyme linked assay (DELA) was carried out in a 96-well format as previously reported [23]. Samples consisted of 6 ng mL^{-1} CTB_5 pentamer conjugated to horseradish peroxidase (CTB-HRP) incubated for 2 hr in the presence of ligand at different concentrations. IC_{50} values were calculated from either duplicate or triplicate data sets of at least ten different concentrations for each ligand by nonlinear regression using the Prism software package (version 3.0, GraphPad Software, Inc.). Reported values are the average of at least two separate experiments.

Protein Expression and Purification

Toxin B pentamers were obtained as described previously [23]. Briefly, wild-type cholera toxin B subunit was expressed by *E. coli* strain Top10 containing a pBAD/CTB_5 vector. The vector is controlled by a pBAD promoter and contains an ampicillin resistance marker. Cells were grown at 30°C in Luria-Bertani Broth (LB) to OD_{600} around 0.4 before overnight induction, initiated by the addition of 0.2% arabinose. Whole-cell lysates were prepared by resuspending the cell pellet in lysis buffer (20 mM Tris-HCl [pH 7.5], 0.1 mM DTT, 0.2 mM EDTA, and 200 mM NaCl) and lysing the cells by two rounds of French press. The supernatant from centrifuged lysate was collected and batch bound to immobilized D-galactose resin (Pierce) for 30 min to 16 hr at 4°C, washed with Buffer G (50 mM Tris-HCl [pH 7.4], 200 mM NaCl, 1 mM EDTA, and 3 mM NaN_3), and eluted with Buffer G + 300 mM D-galactose (Fluka). Residual galactose was removed from purified CTB_5 by dialysis against Buffer G.

Crystallization

Crystals of CTB_5 complexed with BV1 grew from sitting drops containing 1 μl of 30% PEG 300, 50 mM NaCl, and 100 mM Tris-HCl (pH 7.5) mixed with 1 μl of 2.30 mM BV1 mixed with CTB_5 at 5 mg mL^{-1}. The final molar ratio of BV1 to B pentamer was 5:1.

Crystals of CTB_5 complexed with BV2 grew from sitting drops containing 1 μl of 38% PEG 300, 50 mM NaCl, and 100 mM Tris-HCl (pH 7.5) mixed with 1 μl of 2.3 mM BV2 mixed with CTB_5 at 5 mg mL^{-1}. The final molar ratio of BV2 to B pentamer was 5:1.

Crystals of CTB_5 complexed with BV3 grew from sitting drops containing 500 nL of 12% PEG 8000, 50 mM NaCl, 100 mM Tris-HCl (pH 7.5), and 20 mM $MgCl_2$ mixed with 500 nL of 2.3 mM BV3 mixed with CTB_5 at 4.8 mg mL^{-1}. The final molar ratio of BV3 to B pentamer was 5.2:1.

Crystals of CTB_5 complexed with BV4 grew from sitting drops containing 1 μl of 16% PEG 8000, 50 mM NaCl, 100 mM Tris-HCl (pH 7.5), and 20 mM $MgCl_2$ mixed with 1 μl of 2.3 mM BV4 mixed with CTB_5 at 5 mg mL^{-1}. The final molar ratio of BV4 to B pentamer was 5:1.

Mature, well-defined crystals formed within 48 hr of sitting drop preparation and were flash-frozen for collection at the synchrotron light source. Glycerol (30%) in mother liquor was used as a cryoprotectant for the CTB_5:BV3 complex and the CTB_5:BV4 complex. No cryoprotectant was added before flash-freezing the crystals containing BV1 and BV2. All crystals were of space group C2, and had a unit cell that was isomorphous to that of the previously determined structure of CTB_5 complexed with GM1-OS (PDB Accession Number 3chb) [32].

Structure Determination and Refinement

Crystal diffraction data was collected at synchrotron radiation level beamline 8.2.2 at the Advanced Light Source (ALS) at Berkeley National Lab, Berkeley, CA. X-ray diffraction data for CTB_5:BV1 and CTB_5:BV2 were measured at a wavelength of 1.0000 Å. X-ray diffraction data for CTB_5-BV3 was measured at a wavelength of 0.9791 Å. X-ray diffraction data for CTB_5:BV4 was measured at a wavelength of 0.9626 Å. Diffraction images were integrated and scaled with *HKL2000* and *TRUNCATE* [33]. Phases were determined using the molecular replacement program *MOLREP* [34]. CTB_5 complexed with GM1-OS (PDB Accession Number 3chb) with ligand and waters removed, was used as a search model for all data sets.

Rigid body, TLS, isotropic, and anisotropic model refinement were carried out in *REFMAC5* [35] and *ARP/WARP* [36] within the CCP4 suite of programs. Individual anisotropic temperature factors were applied for higher resolution structures BV2, BV3, and BV4 near the end of refinement. Individual anisotropic values varied markedly between subunits. Real-space manual modeling and automated water picking was done with Xfit [37]. A general refinement scheme began with a rigid body refinement, and subsequent restrained refinements while increasing the resolution. Iterative building of the water shell involved automated and manual water placement with *XFIT* and *ARP/WARP* [36] using *SFCHECK* [38] and *WHATCHECK*

[39] along with manual inspection to discern incorrectly modeled waters. TLS parameters and anisotropic refinement parameters for high-resolution structures were then employed during the final rounds of refinement. Partial ligand subtracted maps were used to help refine more "flexible" regions of the ligands. "MNPG subtracted" maps gave good indications of proper piperazine ring placement when applicable. R_{free}, established after scaling, was the quality determinant for all refinement steps. The geometric description of the ligands, TRIS molecule, and PEG fragment for refmac ("cif" file) were generated by feeding a ligand-coordinate file to the website http://davapc1.bioch.dundee.ac.uk/prodrg. The output cif file was then manually inspected with reference to the Cambridge Structural Database before being used in *REFMAC5*.

Acknowledgments

This work was supported in part by the National Institutes of Health (grant AI44954 to E.F. and AI34501 to W.G.J.H.). We gratefully acknowledge the staff of beamline 8.2.2 at the Advanced Light Source for assistance in data collection.

Received: January 29, 2004
Revised: May 17, 2004
Accepted: June 9, 2004
Published: September 17, 2004

References

1. Mammen, M., Choi, S.K., and Whitesides, G.M. (1998). Polyvalent interactions in biological systems: Implications for design and use of multivalent ligands and inhibitors. Angew. Chem. (Int. Edit.) *37*, 2755–2794.
2. Kiessling, L.L., Strong, L.E., and Gestwicki, J.E. (2000). Principles for multivalent ligand design. Annu. Rep. Med. Chem. *35*, 321–330.
3. Hubble, J. (1999). A model of multivalent ligand-receptor equilibria which explains the effect of multivalent binding inhibitors. Mol. Immunol. *36*, 13–18.
4. Gargano, J.M., Ngo, T., Kim, J.Y., Acheson, D.W.K., and Lees, W.J. (2001). Multivalent inhibition of AB(5) toxins. J. Am. Chem. Soc. *123*, 12909–12910.
5. Kitov, P.I., and Bundle, D.R. (2003). On the nature of the multivalency effect: a thermodynamic model. J. Am. Chem. Soc. *125*, 16271–16284.
6. Burke, S.D., Zhao, Q., Schuster, M.C., and Kiessling, L.L. (2000). Synergistic formation of soluble lectin clusters by a templated multivalent saccharide ligand. J. Am. Chem. Soc. *122*, 4518–4519.
7. Dimick, S.M., Powell, S.C., McMahon, S.A., Moothoo, D.N., Naismaith, J.H., and Toone, E.J. (1999). On the meaning of affinity: cluster glycoside effects and concanavalin A. J. Am. Chem. Soc. *121*, 10286–10296.
8. Wright, D., and Usher, L. (2001). Multivalent binding in the design of bioactive compounds. Curr. Org. Chem. *5*, 1107–1131.
9. Pang, Y.P., Kollmeyer, T.M., Hong, F., Lee, J.C., Hammond, P.I., Haugabouk, S.P., and Brimijoin, S. (2003). Rational design of alkylene-linked bis-pyridiniumalidoximes as improved acetylcholinesterase reactivators. Chem. Biol. *10*, 491–502.
10. Wong, D.M., Greenblatt, H.M., Dvir, H., Carlier, P.R., Han, Y.F., Pang, Y.P., Silman, I., and Sussman, J.L. (2003). Acetylcholinesterase complexed with bivalent ligands related to huperzine A: experimental evidence for species-dependent protein-ligand complementarity. J. Am. Chem. Soc. *125*, 363–373.
11. Han, Y.F., Li, C.P.L., Chow, E., Wang, H., Pang, Y.P., and Carlier, P.R. (1999). Dual-site binding of bivalent 4-aminopyridine- and 4-aminoquinoline-based aChE inhibitors: contribution of the hydrophobic alkylene tether to monomer and dimer affinities. Bioorg. Med. Chem. *7*, 2569–2575.
12. Tamiz, A.P., Bandyopadhyay, B.C., Zhang, J.R., Flippen-Anderson, J.L., Zhang, M., Wang, C.Z., Johnson, K.M., Tella, S., and Kozikowski, A.P. (2001). Pharmacological and behavioral analysis of the effects of some bivalent ligand-based monoamine reuptake inhibitors. J. Med. Chem. *44*, 1615–1622.
13. Abadi, A.H., Lankow, S., Hoefgen, B., Decker, M., Kassack, M.U., and Lehmann, J. (2002). Dopamine/serotonin receptor ligands, part III: synthesis and biological activities of 7,7′-alkylene-bis-6,7,8,9,14,15-hexahydro-5h-benz D indolo 2,3-g azecines-application of the bivalent ligand approach to a novel type of dopamine receptor antagonist. Arch. Pharm. *335*, 367–373.
14. Glick, G.D., Toogood, P.L., Wiley, D.C., Skehel, J.J., and Knowles, J.R. (1991). Ligand recognition by influenza virus: the binding of bivalent sialosides. J. Biol. Chem. *266*, 23660–23669.
15. Kitov, P.I., Shimizu, H., Homans, S.W., and Bundle, D.R. (2003). Optimization of tether length in nonglycosidically linked bivalent ligands that target sites 2 and 1 of a shiga-like toxin. J. Am. Chem. Soc. *125*, 3284–3294.
16. Lundquist, J.J., Debenham, S.D., and Toone, E.J. (2000). Multivalency effects in protein-carbohydrate interaction: the binding of the shiga-like toxin 1 binding subunit to multivalent c-linked glycopeptides. J. Org. Chem. *65*, 8245–8250.
17. Fan, E., Merritt, E.A., Verlinde, C., and Hol, W.G.J. (2000). AB(5) toxins: structures and inhibitor design. Curr. Opin. Struct. Biol. *10*, 680–686.
18. Spangler, B.D. (1992). Structure and function of cholera toxin and the related *escherichia coli* heat-labile enterotoxin. Microbiol. Rev. *56*, 622–647.
19. Dewolf, M.J.S., Dams, E., and Dierick, W.S.H. (1994). Interaction of a cholera-toxin derivative containing a reduced number of receptor-binding sites with intact-cells in culture. Biochimica Et Biophysica Acta-Molecular Cell Research *1223*, 296–305.
20. Fan, E., Zhang, Z., Minke, W.E., Hou, Z., Verlinde, C.L.M.J., and Hol, W.G.J. (2000). High affinity pentavalent ligands of *escherichia coli* heat-labile enterotoxin by modular structure-based design. J. Am. Chem. Soc. *122*, 2663–2664.
21. Merritt, E.A., Zhang, Z., Pickens, J., Ahn, M., Hol, W., and Fan, E. (2002). Characterization and crystal structure of a high-affinity pentavalent receptor-binding inhibitor for cholera toxin and *E. coli* heat-labile enterotoxin. J. Am. Chem. Soc. *124*, 8818–8824.
22. Zhang, Z.S., Merritt, E.A., Ahn, M., Roach, C., Hou, Z., Verlinde, C., Hol, W.G.J., and Fan, E. (2002). Solution and crystallographic studies of branched multivalent ligands that inhibit the receptor-binding of cholera toxin. J. Am. Chem. Soc. *124*, 12991–12998.
23. Minke, W.E., Roach, C., Hol, W., and Verlinde, C.L. (1999). Structure-based exploration of the ganglioside GM1 binding sites of *escherichia coli* heat-labile enterotoxin and cholera toxin for the discovery of receptor antagonists. Biochemistry *38*, 5684–5692.
24. Pickens, J., Merritt, E.A., Ahn, M., Verlinde, C.L., Hol, W., and Fan, E. (2002). Anchor-based design of improved receptor-binding antagonists of cholera toxin and *escherichia coli* heat-labile enterotoxin that display multiple binding modes. Chem. Biol. *9*, 215–224.
25. Mitchell, D., Pickens, J., Korotkov, K., Fan, E., and Hol, W.G.J. (2004). 3,5-substituted phenylgalactosides as leads in designing effective cholera toxin antagonists: Synthesis and crystallographic studies. Bioorg. Med. Chem. *12*, 907–920.
26. Knoll, D., and Hermans, J. (1983). Polymer-protein interactions-comparison of experiment and excluded volume theory. J. Biol. Chem. *258*, 5710–5715.
27. Merritt, E.A., Sarfaty, S., Feil, I.K., and Hol, W.G.J. (1997). Structural foundation for the design of receptor antagonists targeting *escherichia coli* heat-labile enterotoxin. Structure *5*, 1485–1499.
28. Merritt, E.A., and Hol, W.G.J. (1995). AB(5) toxins. Curr. Opin. Struct. Biol. *5*, 165–171.
29. Mammen, M., Dahmann, G., and Whitesides, G.M. (1995). Effective inhibitors of hemagglutination by influenza-virus synthesized from polymers having active ester groups-insight into mechanism of inhibition. J. Med. Chem. *38*, 4179–4190.
30. Sigal, G.B., Mammen, M., Dahmann, G., and Whitesides, G.M. (1996). Polyacrylamides bearing pendant α-sialoside groups strongly inhibit agglutination of erythrocytes by influenza virus: the strong inhibition reflects enhanced binding through cooperative polyvalent interactions. J. Am. Chem. Soc. *118*, 3789–3800.
31. Choi, S.K., Mammen, M., and Whitesides, G.M. (1997). Generation and in situ evaluation of libraries of poly(acrylic acid) presenting sialosides as side chains as polyvalent inhibitors of

influenza-mediated hemagglutination. J. Am. Chem. Soc. *119*, 4103–4111.
32. Merritt, E.A., Kuhn, P., Sarfaty, S., Erbe, J.L., Holmes, R.K., and Hol, W.G.J. (1998). The 1.25 angstrom resolution refinement of the cholera toxin B-pentamer: evidence of peptide backbone strain at the receptor-binding site. J. Mol. Biol. *282*, 1043–1059.
33. Otwinowski, Z., and Minor, W. (1997). Processing of x-ray diffraction data collected in oscillation mode. Macromolecular crystallography *276*, 307–326.
34. Vagin, A., and Teplyakov, A. (1997). Molrep: an automated program for molecular replacement. J. Appl. Crystallogr. *30*, 1022–1025.
35. Murshudov, G.N., Vagin, A.A., and Dodson, E.J. (1997). Refinement of macromolecular structures by the maximum-likelihood method. Acta Crystallogr. Sect. D-Biol. Crystallogr. *53*, 240–255.
36. Perrakis, A., Morris, R., and Lamzin, V.S. (1999). Automated protein model building combined with iterative structure refinement. Nat. Struct. Biol. *6*, 458–463.
37. McRee, D.E. (1999). Xtalview xfit-a versatile program for manipulating atomic coordinates and electron density. J. Struct. Biol. *125*, 156–165.
38. Vaguine, A.A., Richelle, J., and Wodak, S.J. (1999). Sfcheck: a unified set of procedures for evaluating the quality of macromolecular structure-factor data and their agreement with the atomic model. Acta Crystallogr. Sect. D-Biol. Crystallogr. *55*, 191–205.
39. Hooft, R.W.W., Vriend, G., Sander, C., and Abola, E.E. (1996). Errors in protein structures. Nature *381*, 272–272.
40. Merritt, E.A., and Bacon, D.J. (1997). Raster3d: photorealistic molecular graphics. Method. Enzymol. *277*, 505–524.

Accession Numbers

Crystal structure coordinates for BV1, BV2, BV3, and BV4 in complex with the B pentamer of cholera toxin have been deposited in the Protein Data Bank (PDB Accession Numbers 1rcv, 1rd9, 1rdp, and 1rf2, respectively).